THE BELL SYSTEM TECHNICAL JOURNAL
Vol. 59, No. 7, September 1980
Printed in U.S.A.

An Exact Numerical Solution to Maxwell's Equations for Lightguides

By G. E. PETERSON, A. CARNEVALE, U. C. PAEK, and D. W. BERREMAN

(Manuscript received December 29, 1979)

To develop a sound base on which to design efficient lightguides, it is necessary to understand the physics of the propagating modes of this new and important transmission medium. To achieve this end, we have calculated numerical solutions to the vector form of Maxwell's equations for lightguides and have obtained all six components of the electromagnetic field. We have included materials dispersion and calculated Poynting vectors and effective and group indices.

I. INTRODUCTION

A possible first step in analyzing production line MCVD (modified chemical vapor deposition) lightguide preforms[1] is to calculate the effective indices for a propagating wave in a fiber assumed to be produced from the preform. A knowledge of the effective indices for various wavelengths permits one to calculate the group indices. Using these, we can calculate the group delay of the modes. In this way, we can ascertain the reproducibility of the preforms and ultimately increase yields of the products.

The solution of Maxwell's equations for a radially inhomogeneous medium such as is found in lightguides is by no means easy. This is because we must deal with fourth-order differential equations with variable coefficients. Various approximations can, of course, be made.[2-8] For example, a popular one is to neglect the gradient of the logarithm of the dielectric constant with respect to radial distance[9] and then employ WKB methods.[10]

These approximations require that discontinuities in index be of little importance and that the refractive index vary slowly with distance. Solutions of this sort have had a substantial impact on lightguide engineering.[11]

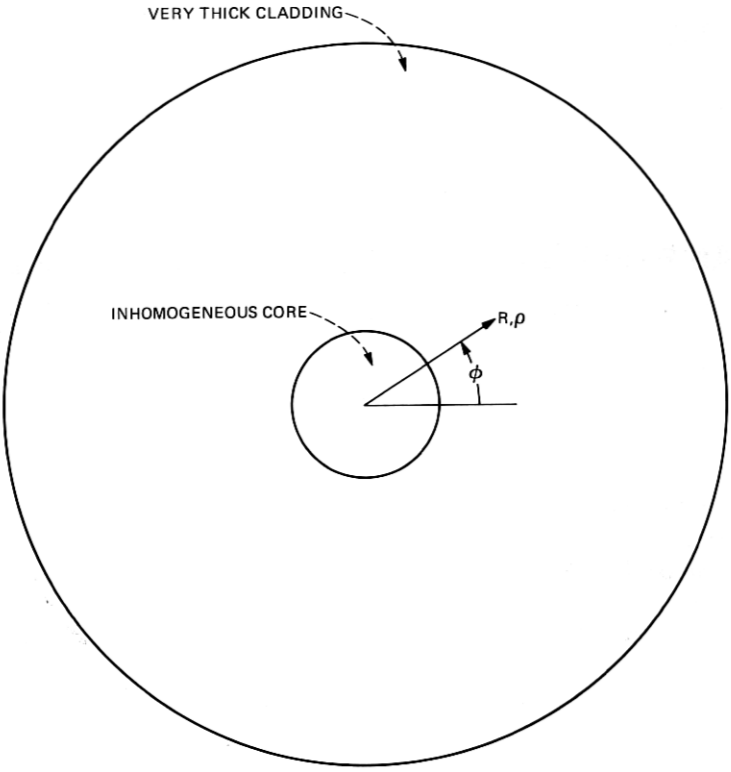

Fig. 1—Schematic diagram of a lightguide showing an inhomogeneous core and a very thick (essentially infinite) cladding. R or ρ is the radial coordinate, and ϕ is the polar angle ($\rho = K_o R$).

If we cannot or do not wish to limit ourselves to the restrictions imposed by these approximations, we have little choice but to keep Maxwell's equations intact and resort to numerical techniques. For example, Vigants and Schlesinger[12] have analyzed microwave surface waves on radially inhomogeneous cylinders using numerical procedures. In a like manner, Vassel[13] has studied SELFOC[14] optical waveguides.

In this paper, we extend these methods and apply them to the analysis of idealized lightguides. In particular, we examine those aspects of the physics of lightguides that are most clearly elucidated by the numerical solutions. We shall apply these methods to production-line preforms and lightguides in subsequent papers.

A choice of wavelengths and fiber diameters to study in the present paper is necessary. From a purely engineering point of view, a 50-micron-diameter fiber and wavelengths of 0.6328, 0.820, 0.850, 1.30 and 1.55 microns would be essential. This diameter and these wavelengths

will be applied to all production-line preforms and lightguides analyzed in future work. A very large fiber (300 microns) with very many modes would be a severe test of our numerical analysis, but would be of little practical interest.

A compromise is clearly necesary. We have chosen to study a 100-micron-diameter fiber. This adequately tests our programs and our ability to handle many modes. As we are interested in this paper in rather uniformly spaced wavelengths, our choice of wavelengths does not coincide exactly with those of engineering importance.

II. THEORY

We consider a cylindrical lightguide with an inhomogeneous core and a thick (essentially infinite) cladding (see Fig. 1). The bound propagating modes in the core will be of the form:

$$\Gamma(R) \exp i[\omega t - M\phi - K_o N_e Z]. \tag{1}$$

Here ϕ is the polar angle, M the azimuthal mode number, Z the longitudinal coordinate, R the radial coordinate, K_o the free-space propagation parameter, and N_e the effective refractive index of the wave.

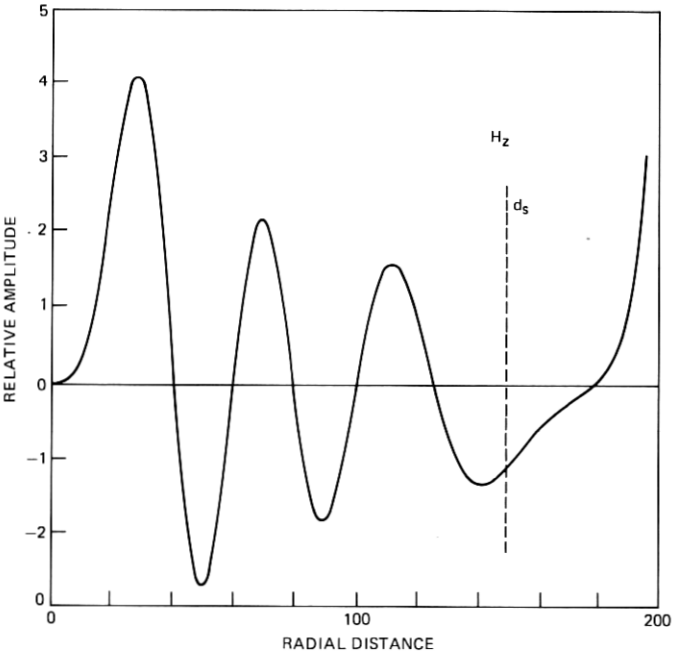

Fig. 2—A possible solution to eq. (2) for H_z. To the left of the line d_s, the solution is purely oscillatory. To the right of the line, it is the sum of a rising and decaying exponential. In this plot, $M = 4$.

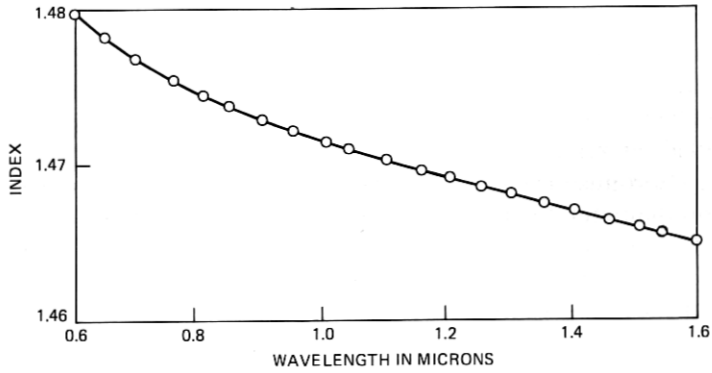

Fig. 3—The wavelength variation of refractive index of 13.5-mole-percent germania-doped silica.

Maxwell's equations in cylindrical coordinates can be rigorously written as[6,7,15]

$$\frac{d\Gamma}{d\rho} = \rho^{-1}A(\rho)\Gamma(\rho). \tag{2}$$

Here $\Gamma(\rho)$ is a column vector whose four elements are related to the tangential components of the electromagnetic field. These components will be continuous through the core-cladding interface. They are as follows:

$$\begin{aligned} \Gamma_1 &= E_z \\ \Gamma_2 &= -i\,\rho\,H_\phi Z_o \\ \Gamma_3 &= \rho E_\phi \\ \Gamma_4 &= -iH_z Z_o, \end{aligned} \tag{3}$$

where Z_o is the wave impedance of free space and the variable ρ is defined as $K_o R$.

The 4×4 matrix $A(\rho)$ can be written as:

$$\begin{vmatrix} 0 & (N_e^2/\kappa) - 1 & 0 & -MN_e/\kappa \\ \rho\kappa - M^2 & 0 & MN_e & 0 \\ 0 & MN_e/\kappa & 0 & \rho^2 - (M^2/\kappa) \\ -MN_e & 0 & N_e^2 - \kappa & 0 \end{vmatrix} . \tag{4}$$

In this matrix, κ is the dielectric constant that varies throughout the core of the fiber and remains constant in the cladding. In general, κ will be expected to change with frequency ω.

It can be shown[12,13] that, as $\rho \to \infty$, we obtain a form of Bessel's equation. For decaying solutions in the cladding, we consequently employ modified Bessel functions of the second kind $K_M(\xi)$. There will be two independent solution vectors in the cladding. They are[13]

$$W_M(\xi) \cdot \begin{bmatrix} N_e^2 - \kappa(c) \\ \kappa(c)\gamma_m(\xi) \\ MN_e \\ 0 \end{bmatrix} \quad \text{and} \quad W_M(\xi) \cdot \begin{bmatrix} 0 \\ MN_3 \\ \gamma_m(\xi) \\ N_e^2 - \kappa(c) \end{bmatrix}. \tag{5}$$

Here $\kappa(c)$ is the dielectric constant in the cladding and

$$\begin{aligned} \xi &= [N_e^2 - \kappa(c)]^{1/2}\rho_{cc} \\ W_M(\xi) &= [N_e^2 - \kappa(c)]^{-4}K_M(\xi) \\ \gamma_M(\xi) &= \xi\, K_M'(\xi)/K_M(\xi), \end{aligned} \tag{6}$$

where ρ_{cc} is the ρ value at the core-cladding interface.

To find the solution vectors in the core, we make the following change in variable in eq. (2):

$$\Gamma = \rho^M \Lambda. \tag{7}$$

We thus obtain the differential equation,

$$\frac{d\Lambda}{d\rho} = \frac{1}{\rho}[A(\rho) - MI]\Lambda, \tag{8}$$

where I is a unit diagonal matrix.

By requiring that the solution be bounded as $\rho \to o$, we obtain the two vectors,[13]

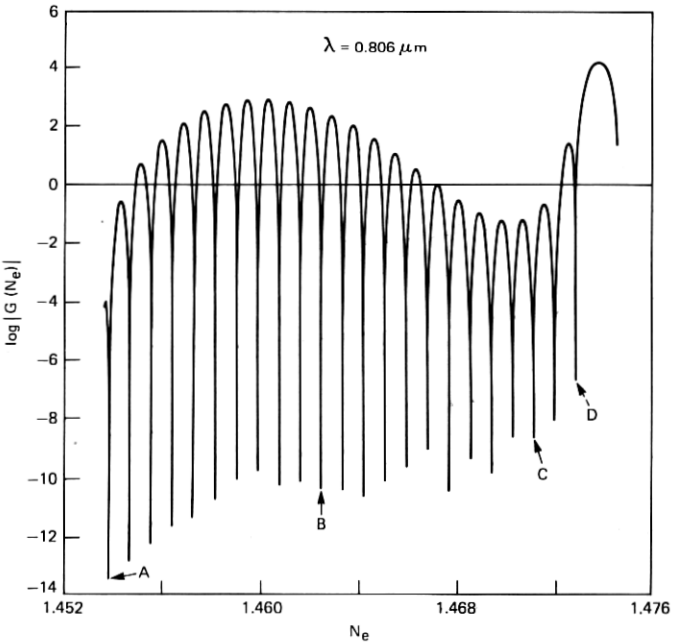

Fig. 4—Plot of the function $\log |\, G(N_e)\,|$ versus effective index for $M = 4$ and $\lambda = 0.806$ micron. The index profile is parabolic.

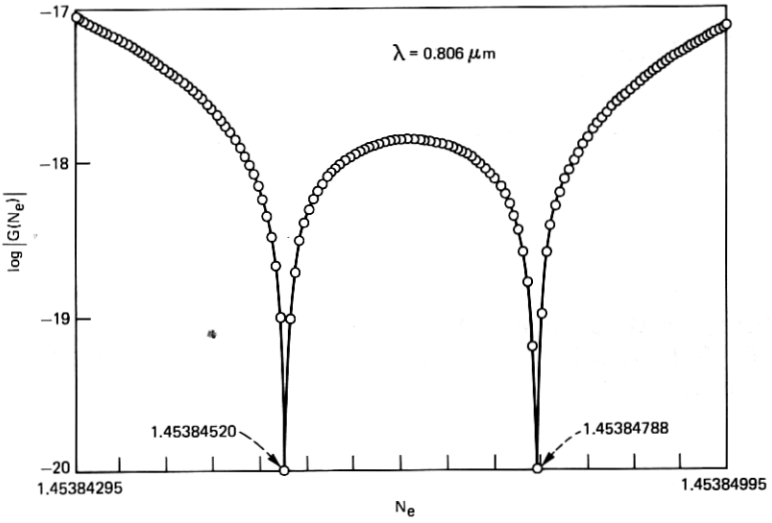

Fig. 5—A high resolution plot of $\log|G(N_e)|$ for the mode marked A in Fig. 4. This splitting is due to the presence of the cladding and amounts to a few times 10^{-6}.

$$\begin{bmatrix} N_e^2 - \kappa(o) \\ M\kappa(o) \\ MN_e \\ 0 \end{bmatrix} \quad \text{and} \quad \begin{bmatrix} 0 \\ MN_e \\ M \\ N_e^2 - \kappa(o) \end{bmatrix}, \tag{9}$$

where $\kappa(o)$ is the dielectric constant at the center of the lightguide.

By using the two solution vectors at the center of the lightguide and eq. (8), we can obtain two numerical solutions at the core-cladding interface. These must match with the two cladding solutions at the same point. This can be written as

$$\sum_{i,j} \Gamma_{ij}(\rho_{cc}, N_e)\, P_j = o, \tag{10}$$

where index j specifies a particular vectors and index i a particular vector component. Consequently, $\Gamma_{i,1}$ and $\Gamma_{i,2}$ are core solutions and $\Gamma_{i,3}$ and $\Gamma_{i,4}$ are cladding solutions. P_1 and P_2 are the weights applied to the core solutions, and P_3 and P_4 are the weights applied to the cladding solutions. The characteristic equation from which we can determine N_e can then be written as

$$G(N_e) = \mathrm{Det}[\Gamma_{i,j}(\rho_{cc}, N_e)] = o. \tag{11}$$

This is an implicit, transcendental equation, and to find its solution we plot $G(N_e)$ as a function of N_e. The zeros will give us the allowed values of effective index.

III. COMPUTING PROCEDURE

We obtain numerical solutions to eq. (8) by means of an optimized second-order Runge-Kutta procedure.[16] Double-precision arithmetic is employed and needed. To minimize computing time, we wrote our own programs especially tailored to the above problem.

There will be regions in the lightguide where the solution to eq. (2) will oscillate and other regions where the solution will grow or decay exponentially. As we are limited by our computer to numbers between 10^{-38} to 10^{+38}, this will limit the wavelength and size of the fiber we can study. However, as will be seen, realistic fibers and wavelengths can

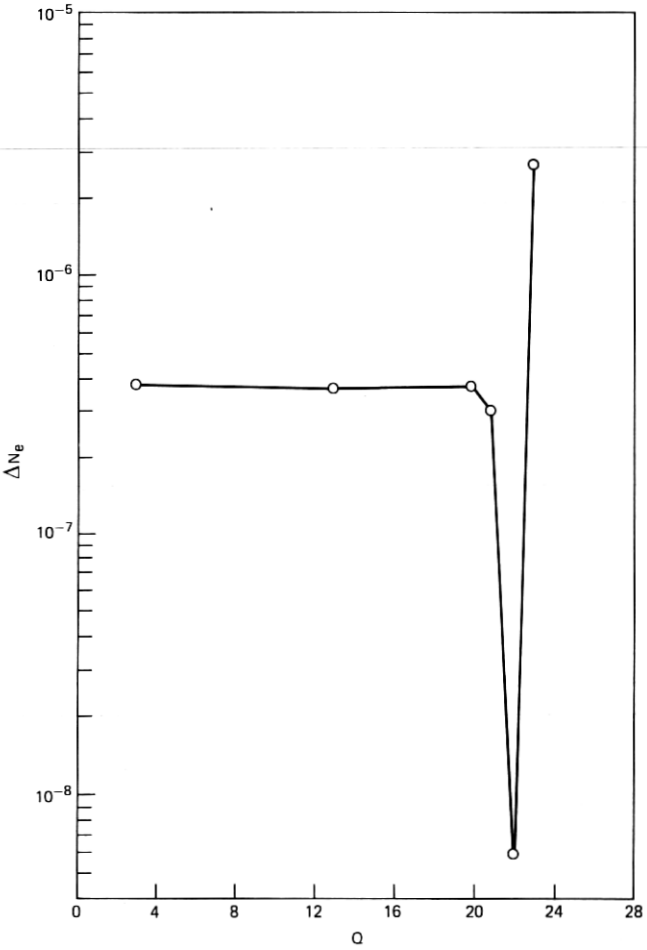

Fig. 6—A plot of the absolute value of the splitting of the modal pairs vs mode number Q. The dramatic change in splitting for $Q = 22$ and 23 is due to the cladding.

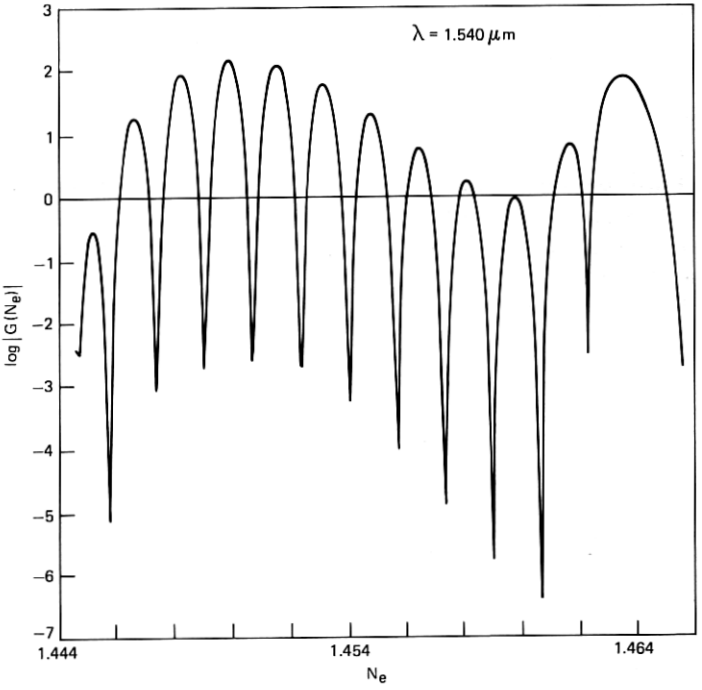

Fig. 7—Plot of the function $\log|G(N_e)|$ vs effective index for $M = 4$ and $\lambda = 1.540$ microns. Note the increase in spacing between the effective indices over the data on Fig. 4.

be handled. As an illustration, Fig. 2 shows a possible solution to eq. (2) for H_z. To the left of the vertical line d_s, the behavior is clearly oscillatory. To the right of the line, we have the sum of a rising and decaying exponential. The decaying term dominates nearest the line, while the rising term dominates further away. The line d_s locates the turning point, and it should not be confused with the core-cladding interface. It is simply that radial position where the character of the solution changes from oscillatory to exponential. For loosely bound modes, it will be very near the core-cladding interface. For tightly bound modes, it will be near the center of the lightguide.

As mentioned before, the solution in the cladding can be written in terms of modified Bessel functions of the second kind. We obtain these functions by a double-precision routine written by Gatto and Seery.[17] Again, because of the range of numbers the computer can handle, there is some limitation on the size of the argument the program can evaluate. However, realistic wavelengths and fiber diameters are not precluded.

The function $G(N_e)$ that we must plot to obtain the N_e's (i.e.,

effective indices) has a large dynamic range. We are primarily interested in the zeros of this function. The large values can be compressed by plotting the logarithms of the absolute values of $G(N_e)$. It should be borne in mind that exact zeros for $|G(N_e)|$ are not very likely, as $G(N_e)$ is the result of a numerical calculation. What we find are approaches to zero, and this causes no difficulty as these approaches are very evident.

IV. EFFECTIVE INDICES FOR AN IDEALIZED FIBER

We study an idealized lightguide with a 13.5-mole percent germania-doped silica core and a pure silica cladding. The core is assumed to be perfectly cylindrical with a diameter of 100 microns. The cladding will be considered essentially infinite. The doping profile is such that the refractive index is a parabolic function of distance R. Thus,

$$N = N_1 + \frac{N_2 - N_1}{R_{cc}^2} R^2, \tag{12}$$

where N_1 is the refractive index at the center of the core, N_2 the

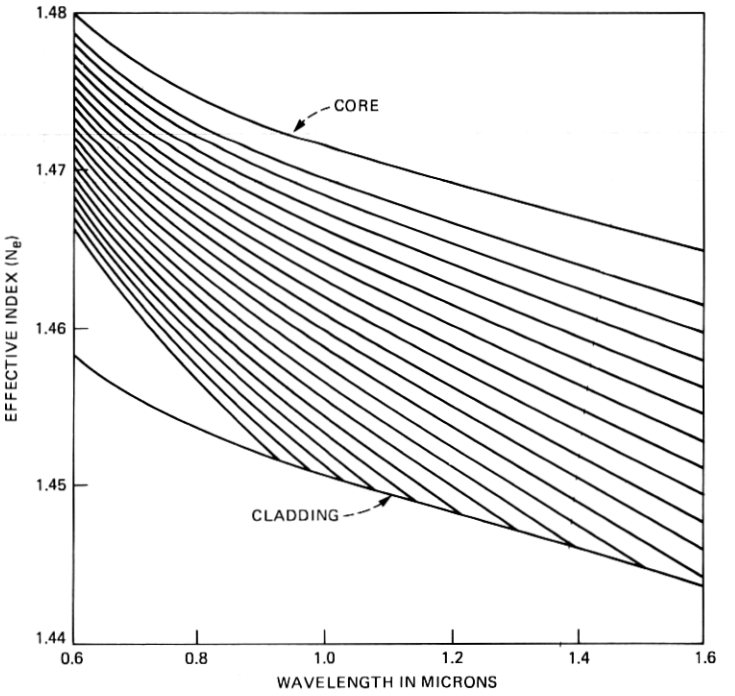

Fig. 8—A family of dispersion curves for the various modes. The curves for the core and cladding are also drawn. Modes that touch the cladding curve are no longer bound to the core.

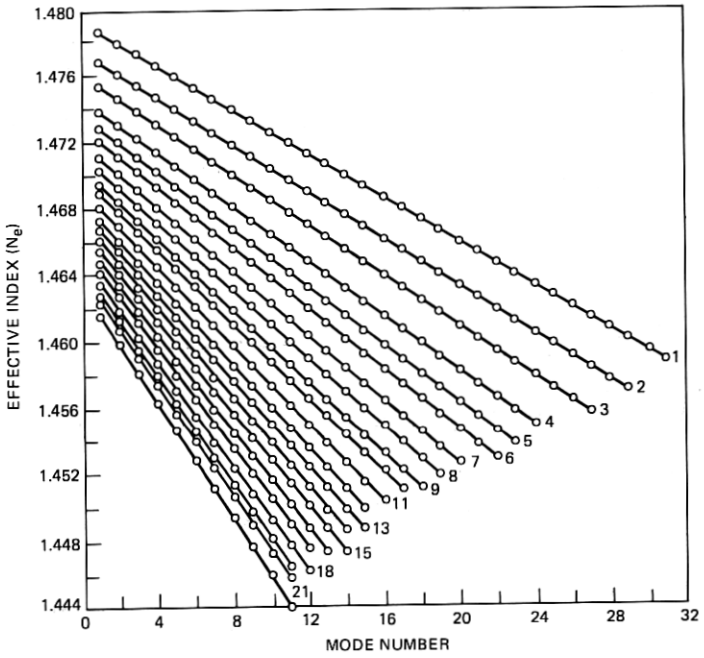

Fig. 9—A plot of effective index vs mode number Q. This highly linear behavior is only for purely parabolic index profile.

refractive index in the cladding, and R_{cc} the radius of the core. Both N_1 and N_2 will be functions of wavelength.

Fleming[18,19] has accurately determined the wave-length variation of the refractive index of silica and some doped silicas. The data for 13.5-mole percent germania-doped silica is shown in Fig. 3. As expected, the refractive index falls off slowly with wavelength.

It is necessary to have a formula for the wave-length dependence of index data such as is shown in Fig. 3. One which is linear in its constants is[20]

$$N_i = C_0 + C_1\lambda^2 + C_2\lambda^4 + C_3/(\lambda^2 - 0.035) + C_4/(\lambda^2 - 0.035)^2 + C_5/(\lambda^2 - 0.035)^3, \quad (13)$$

where λ is in microns and $i = 1, 2$. We find that this formula fits the data of Fig. 3 with a correlation coefficient[21] of 0.9999. Table I lists the coefficients for eq. (1) for both 13-mole-percent germania-doped silica and silica.

There is a physical interpretation of eq. (13). The first terms are a Taylor series corresponding to the influence of a far infrared band. The last terms are a Laurent series corresponding to an absorption band near $\lambda = 1870$Å. We find that this formula is also useful in fitting

Table I—Coefficients for eq. (13) for core and cladding

	Core*	Cladding*
$C_0 =$	1.4706868	1.4508554
$C_1 =$	−0.0026870	−0.0031268
$C_2 =$	−0.0000356	−0.0000381
$C_3 =$	0.0035756	0.0030270
$C_4 =$	−0.0000828	−0.0000779
$C_5 =$	0.0000018	0.0000018

* The deviation of any index from the fitted curve is less than 10^{-7}.

the effective index data for the various modes. For this application, the correlation coefficient is equally good.

Figure 4 shows a plot of the $\log | G(N_e) |$ vs effective index for our idealized fiber with $M = 4$ and $\lambda = 0.806$ micron. We notice that there are 23 clear approaches to zero, and these are the allowed values of N_e. The spacing between the N_e values is essentially uniform, and they span a range from the core center index (1.47453235) to the cladding index (1.4535429).

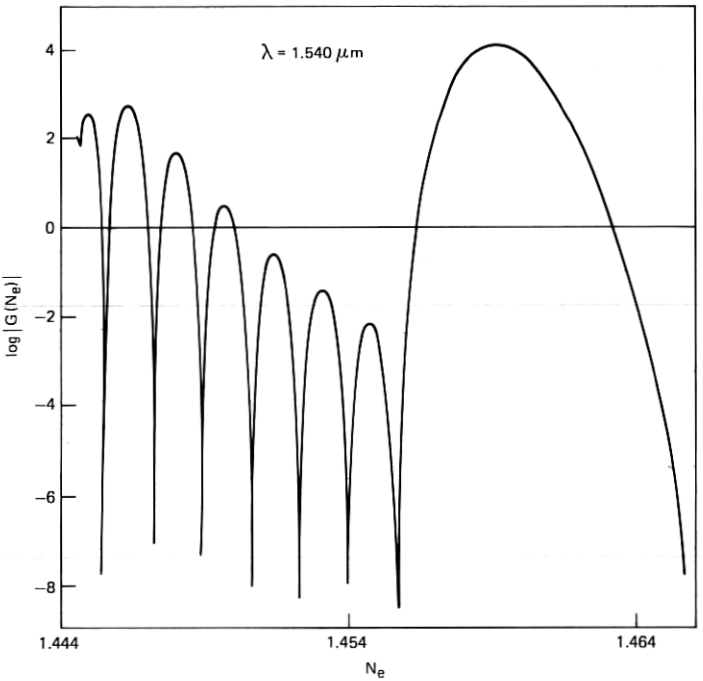

Fig. 10—Plot of the function $\log | G(N_e) |$ vs effective index for $M = 12$ and $\lambda = 1.540$. A comparison with Fig. 7 shows a gap in the allowed effective index values. As M gets even larger, the gap will increase further.

Table II—Listing of the wavelengths* used in Figs. 8 and 9

I	λ_I (microns)
1	0.6040
2	0.6520
3	0.7000
4	0.7600
5	0.8060
6	0.8480
7	0.9020
8	0.9500
9	1.0040
10	1.0400
11	1.1000
12	1.1560
13	1.2020
14	1.2520
15	1.2980
16	1.3520
17	1.4000
18	1.4556
19	1.5040
20	1.5400
21	1.6000

* Rounded from double precision values.

If we examine the approaches to zero under higher resolution than is shown in Fig. 4, we find that, except for the mode marked D, the allowed values of N_e are doublets. Figure 5 shows a high resolution plot of $\log|G(N_e)|$ for the mode marked A. The two values of the effective indices are

$$N_e^1 = 1.45384520$$

$$N_e^2 = 1.45384788.$$

The difference between these two values is a few times 10^{-6}. This splitting is due to the presence of the cladding. For example, a mode whose electromagnetic field has decayed before reaching the cladding (such as B in Fig. 4) has a splitting of a few times 10^{-7}. Figure 6 is a plot of the absolute value of this splitting vs mode number Q. Q counts the number of pairs of modes where $Q = 1$ corresponds to the nondegenerate mode D.

From data of the sort shown in Fig. 4 except that they are taken at different wavelengths, it is possible to draw a family of dispersion curves for the effective indices. Figure 7 shows a curve analogous to Fig. 4 except for $\lambda = 1.540$ microns. The only obvious change is that the spacing between the effective indices has increased. We have collected data at 21 wavelengths, and these are listed in Table II. The family of dispersion curves that results from this data is plotted in Fig. 8. Included in the plot are the dispersion curves for the core and

cladding material. Note that the resolution of Fig. 8 is not high enough to show the splitting of the degenerate modes.

There is some similarity in shape between the effective index curves and the core and cladding curves. We also clearly see the increase in spacing between the effective index curves for longer wavelengths. Some modes are seen to approach the curve for the cladding. When this happens, such modes are no longer bound to the core. Plots like Fig. 8 display rather well the characteristics of the lightguide. Another sort of plot of the data of Fig. 8 is also informative. Rather than plotting N_e vs wavelength for a given mode, we can plot N_e vs mode number Q for a given wavelength. Such a plot is shown in Fig. 9, and the wavelengths are those of Table II. The most striking feature is that N_e for a given wavelength is nearly a linear function of Q.

Another important aspect of the basic physics of lightguides is shown in Fig. 10. This plot is identical with Fig. 7, except that M now equals 12. We note that there is a gap in the allowed effective index values. Such a gap also exists in the data of Fig. 7, but it is not nearly so evident. As M increases further, the gap will get larger, until finally all modes are prohibited.

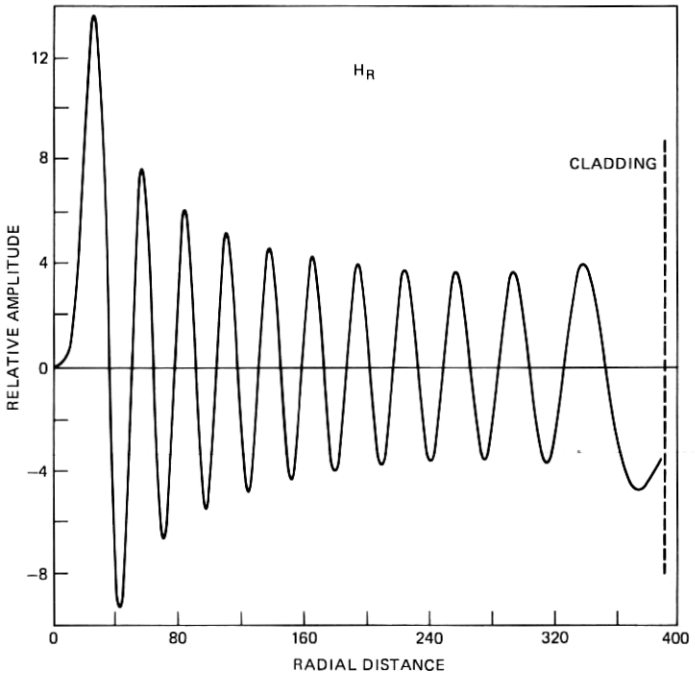

Fig. 11—The H_R wavefunction for $M = 4$ and $\lambda = 0.806$ micron. The effective index is 1.4538452. Only the field in the core is plotted. The radial distance is in terms of ρ. Note that, at the core cladding interface, the field has a substantial value.

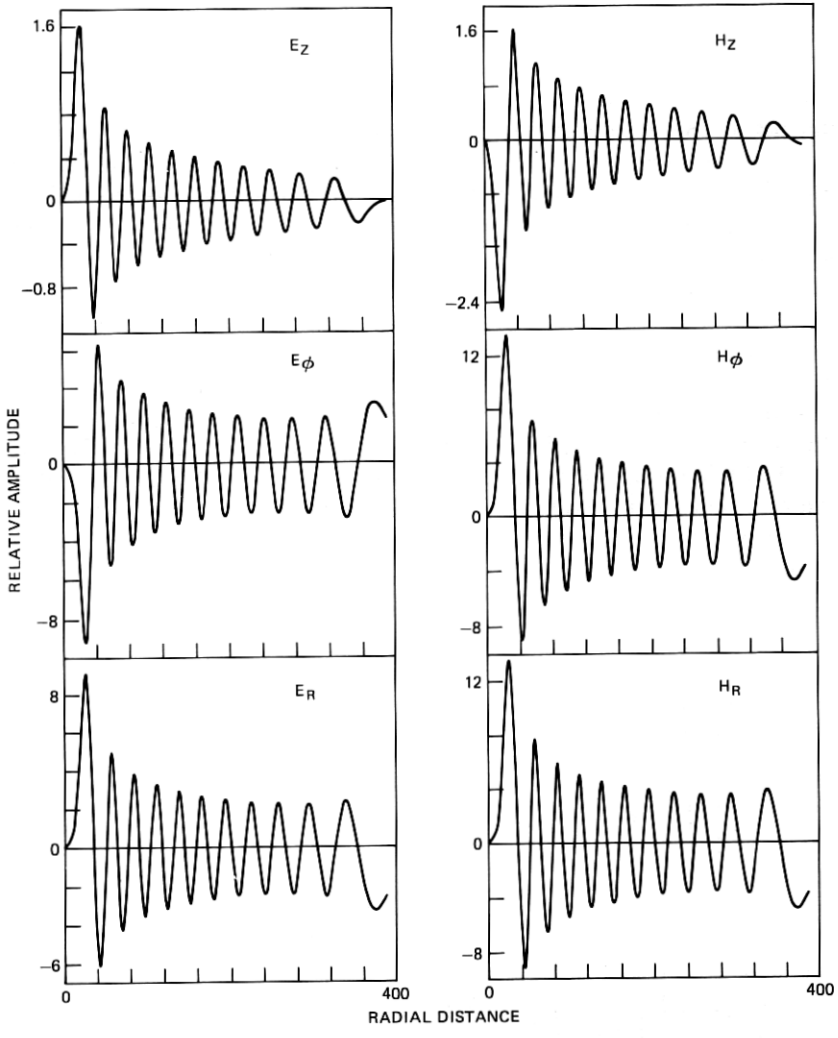

Fig. 12—A plot of all six components of the electromagnetic field. Again $M = 4$, $\lambda = 0.806$, and $N_e = 1.4538452$.

V. WAVEFUNCTIONS FOR THE ELECTROMAGNETIC FIELD

Knowing the effective index for a mode, we can generate the wavefunctions for the electromagnetic field by means of eqs. (3) and (10). We again consider the pair of modes labeled A in Fig. 4. Figure 11 shows the H_R wave-function for the lower of the two effective indices. The radial distance is in terms of the variable ρ. The function plotted corresponds to the field in the core. In the cladding, which is to the right of the dotted line at $\rho = 380$, the field decays in a roughly

exponential manner. Since H_R is not tangential to the core-cladding interface, it will, of course, show a discontinuity at this boundary.

We note a number of features in Fig. 11. First, the field oscillates with decreasing frequency as a function of ρ. Second, the field has a substantial, nonzero value at the core-cladding interface. This means that, for this mode, appreciable energy is carried in the cladding. Finally, we note that the oscillations for this component do not show a continual decrease in amplitude with ρ. There is an initial decrease to a constant level and, just at the core-cladding interface, a slight increase. All six components are shown in Fig. 12. Only E_z and H_z decay continuously with ρ.

From a knowledge of the field functions, the Poynting vector[22] may be calculated. Thus:

$$P = \frac{1}{2}(E_R H_\phi^* - E_\phi H_R^*). \tag{14}$$

This vector, which gives us the power density in the guide, is plotted vs ρ in Fig. 13 for the field functions of Fig. 12. We note a decrease in power from the guide center to a relatively constant level and then an

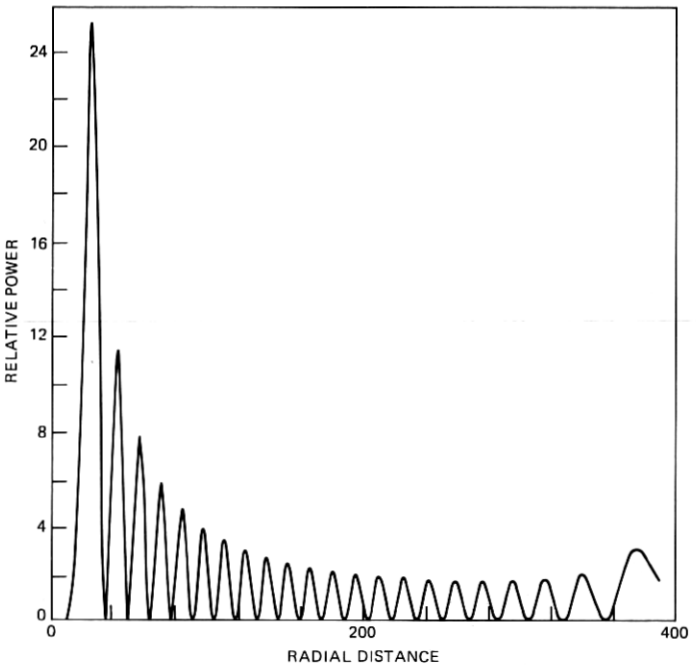

Fig. 13—Poynting vector for the field functions shown in Fig. 12. The vertical scale is relative.

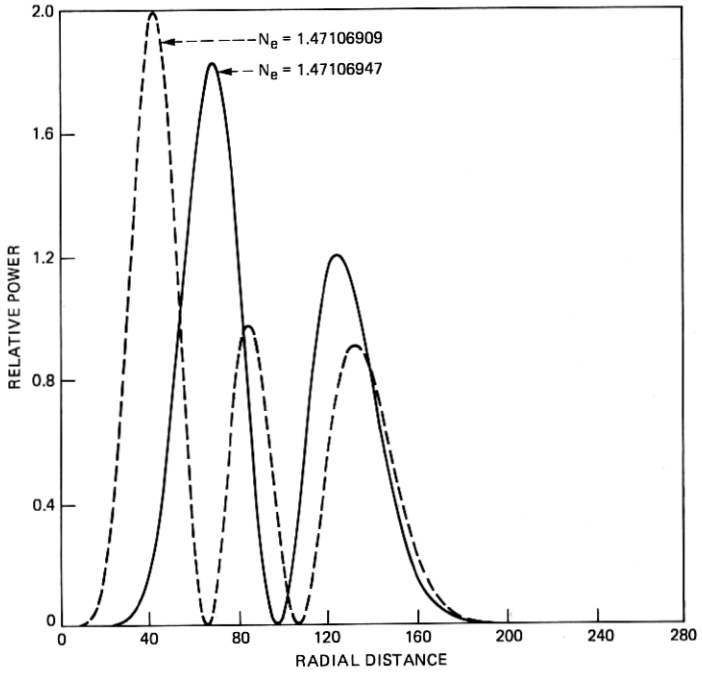

Fig. 14—Poynting vectors for the pair of modes designated C in Fig. 4. We note that one mode has three peaks and the other two. $Q = 3$ for this pair of modes.

increase at the core-cladding interface. We also note an increase in the width of the power peaks as the cladding is approached.

We may use the Poynting vector to classify the more tightly bound modes. By tightly bound, we mean those modes that are little affected by the cladding. Modes with $Q = 1$ through $Q = 20$ (see Fig. 6) are examples of these. To illustrate this classification scheme, consider the pair C, ($Q = 3$) in Fig. 4. The effective indices for these are:

$$N_e^1 = 1.47106909$$

$$N_e^2 = 1.47106947.$$

The Poynting vectors are plotted in Fig. 14 for this pair of modes. The core-cladding interface is well to the right of these functions and is not shown. Obviously, little energy is being carried in the cladding. We see that the mode with the highest efffective index has two peaks and the mode with the lowest has three peaks. We designate the latter mode as HE_{43} and the former EH_{42}. A consistent classification[23] for the two modes of each pair is $HE_{M,Q}$ and $EH_{M,Q-1}$. No EH mode is associated with an $HE_{M,1}$ mode.

VI. CALCULATION OF GROUP INDICES

A parameter of some importance in lightguide engineering is the group index. This will be expected to vary with wavelength and mode. Because many modes will normally be excited and because a source has some spectral width, there will be a spread in group indices ΔN_g. For a fiber of length L, this results in a spread in propagation time Δt given by

$$\Delta t = \frac{L}{C}\Delta N_g. \tag{15}$$

The group index is related to the effective index by

$$N_g = N_e - \lambda(dN_e/d\lambda). \tag{16}$$

This formula may be applied to bulk glass as well, in which case N_e is simply the usual index of refraction. To apply eq. (16), we must calculate $dN_e/d\lambda$ for numerical data, and this could be troublesome. We represent the data on both bulk glass and the effective index of Fig. 8 by eq. (13). The coefficients are determined by a least-squares

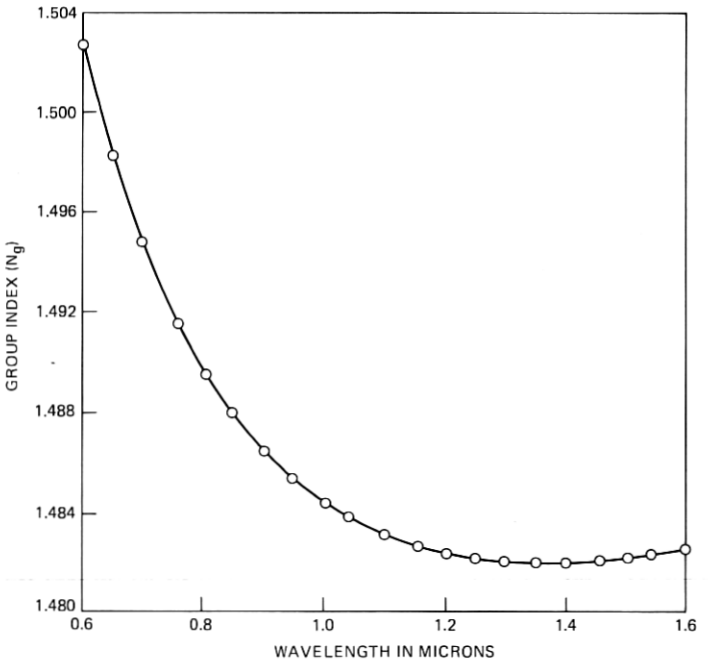

Fig. 15—Group index as a function of wavelength for the bulk germania-doped silica glass whose index of refraction dependence is given in Fig. 3. Note that, near 1.4 microns, there is very little change of group index with wavelength.

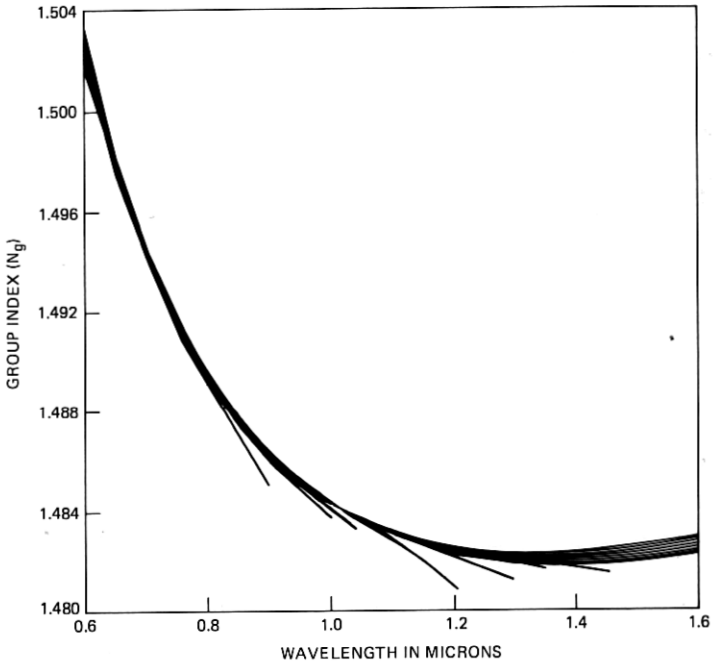

Fig. 16—The family of group index curves for the effective index data of Fig. 8. Note the similarity with the curve of Fig. 15. The curves deviating from the bundle are tending to become unbound.

analysis, and this causes a degree of smoothing. The derivative $dN_e/d\lambda$ is then easily evaluated.

Figure 15 shows the group index as a function of wavelength for the bulk germania-doped glass data shown in Fig. 3. Of course, since we are dealing with bulk glass only, there will be no modal dependence. In the neighborhood of 1.4 microns, there is little change in group index with wavelength. Thus, at this wavelength a rather broad source would transmit data through the bulk material efficiently.

In Fig. 16, we show the family of group index curves for the data of Fig. 7. Each curve corresponds to a particular mode. We note that the modes form a bundle with a shape nearly identical to that of the bulk glass data of Fig. 15. Because of the steepness of the function near 0.8 micron, one tends to get a false impression of the relative width of the bundle. In fact, one finds that it is only slightly wider at the longer wavelengths. The bundle has curves deviating from it, and these are modes that are tending to become unbound. From Fig. 16 we estimate a spread in group index of about 6×10^{-4} at 1.4 microns. The time spread calculated by eq. (15) is thus 2×10^{-9} s/km for a broad source. The bundle shows narrowing at about 1 micron, and this might be a desirable wavelength to operate a narrower source.[11]

VII. GRAPHICAL DISPLAY OF GROUP INDEX

It is useful at times to have a graphical display of group index as a function of effective index. This may be helpful in understanding the effect of distortions in the index profile on differential modal delay. Differentiating eq. (9) yields

$$\frac{\partial G}{\partial \lambda} d\lambda + \frac{\partial G}{\partial N_e} dN_e = 0 \tag{17}$$

$$\text{or} \quad \frac{dN_e}{d\lambda} = -\frac{\partial G}{\partial \lambda} \Big/ \frac{\partial G}{\partial N_e}. \tag{18}$$

Thus we obtain the equation

$$N_g = N_e + \lambda \left(\frac{\partial G}{\partial \lambda} \Big/ \frac{\partial G}{\partial N_e} \right). \tag{19}$$

This function is plotted in Fig. 17 for $\lambda = 1.39$ microns, $M = 4$, and, as before, a parabolic index profile. From Fig. 17, we see that N_g is made up of a family of "dispersion-like curves," and there is one curve for each pair of nearly degenerate modes. For the modes that are little influenced by the cladding, the curves are very similar. The only

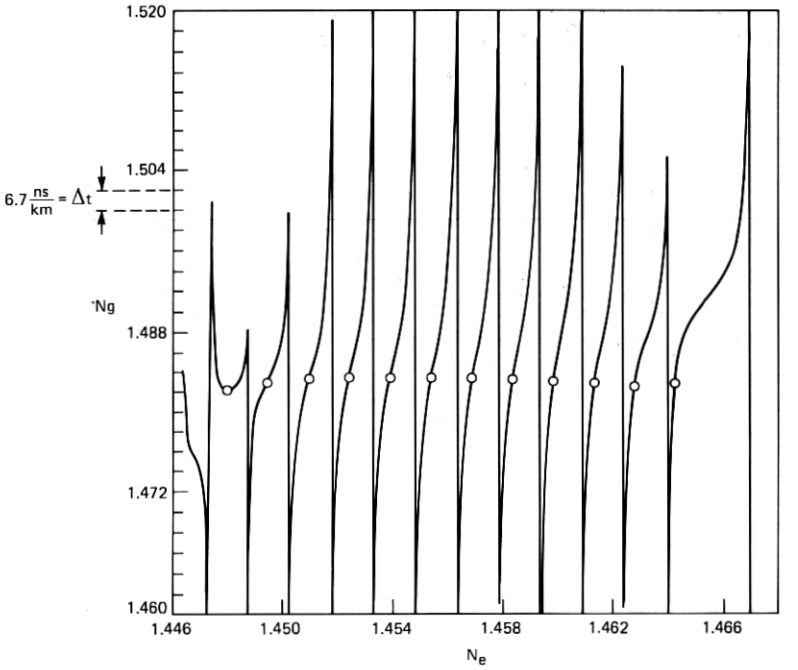

Fig. 17—Plot of eq. (17) relating group index to effective index for $\lambda = 1.39$ microns. The dots correspond to the allowed values of effective index and were taken from plots of the sort shown in Figs. 4 and 7.

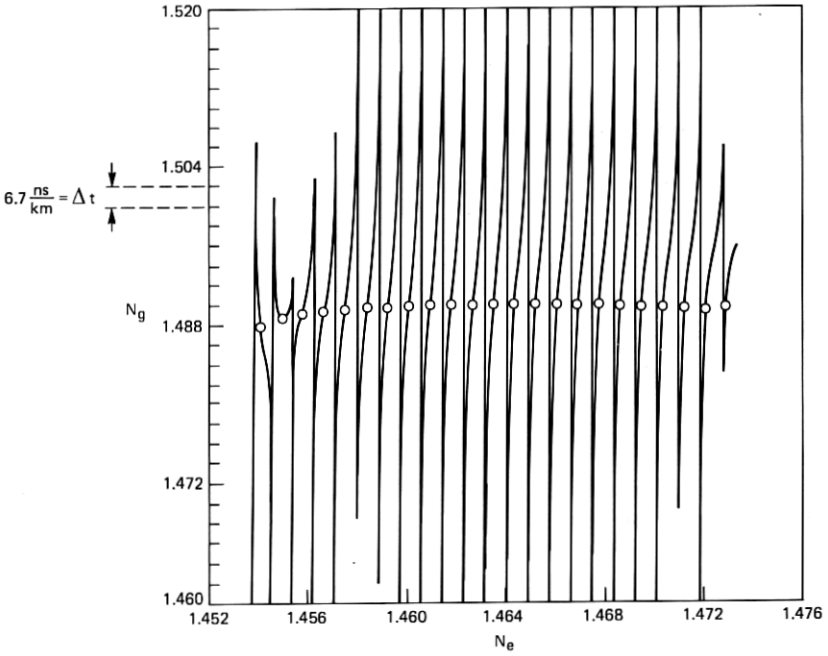

Fig. 18—Plot of eq. (17) relating group index to effective index for $\lambda = 0.803$ micron. The dots correspond to the allowed values of effective index and were taken from plots of the sort shown in Figs. 4 and 7.

difference is a downward shift as N_e gets smaller. For those modes that are influenced by the cladding, i.e., those on the extreme left of the plot, the curves tend to reverse.

The dots on the curves are the values of effective index for each mode. These data were obtained from plots of the sort described earlier (see Figs. 4 and 7). For each mode, we can get a group index. Figure 18 shows a plot for the same fiber except at a shorter wavelength. In this case, we have $\lambda = 0.803$ micron, and there are many more modes. The curves are much steeper and, as before, they change in character as the cladding is approached.

To accurately calculate the group indices at a particular wavelength, one can use either eq. (16) or eq. (19). If we use eq. (16), we must very precisely determine the effective indices for the modes of interest at three equally spaced wavelengths, for example, 0.81, 0.82, and 0.83 microns. The required derivative is then easily evaluated. This is a simple procedure, but has the disadvantage that precise eigenvalues are needed at a number of wavelengths. This is costly in computer time. On the other hand, if we use eq. (19), then we only need to accurately determine the effective indices at one wavelength. The actual calculation of the group index just requires a trivial incrase in

computer time over that needed to accurately determine the effective indices at a single wavelength.[23] The disadvantage of this procedure is that the ratio of two derivatives need be calculated, and this could be less accurate.

VIII. CONCLUSIONS

Using numerical methods, we have obtained solutions to the vector form of Maxwell's equations for idealized lightguides. The results obtained clarify the physics and suggest that application of these methods to production-line preforms and lightguides will be useful. In particular, displays of the effective index data such as shown in Fig. 4 and the displays of group index data such as shown in Fig. 18 may be valuable. In addition to the work described in this paper, we have tested the mathematical methods for step-index, single-mode fibers. Agreement with known results is excellent.

IX. ACKNOWLEDGMENTS

M. I. Cohen and R. J. Klaiber recognized early the importance of solving Maxwell's equations without resorting to WKB and other approximations. Their enthusiasm and encouragement are greatly appreciated. Stimulating discussions with J. W. Fleming concerning dispersion in glass are gratefully acknowledged.

REFERENCES

1. J. B. MacChesney, P. B. O'Connor, and H. M. Presby, "A New Technique for the Preparation of Low-Loss and Graded-Index Optical Fibers," Proc. IEEE, *62* (September 1974), pp. 1280–1281.
2. D. Marcuse, *Light Transmission Optics* New York: Van Nostrand, 1972, Chap. 7.
3. W. Streifer and C. N. Kurtz, "Scalar Analysis of Radially Inhomogeneous Guiding Media," J. Opt. Soc. Am, *57* (June 1967), pp. 779–786.
4. C. N. Kurtz and W. Streifer, "Guided Waves in Inhomogeneous Focusing Media, Part I: Formulation, Solution for Quadratic Inhomogeneity," IEEE Trans., *MTT-17* (January 1969), pp. 11–15.
5. M. Matsuhara, "Analysis of TEM Modes in Dielectric Waveguides, By a Variational Method," J. Opt. Soc. Am., *63* (December 1973), pp. 1514–1517.
6. C. N. Kurtz and W. Streifer, "Guided Waves in Inhomogeneous Focusing Media, Part II: Asymptotic Solution for General Weak Inhomogeneity," IEEE Trans., *MTT-17* (May 1969).
7. J. G. Dil and H. Blok, "Propagation in Graded Index Optical Fibers," Opto-Electronics, *5* (May 1973), pp. 415–420.
8. D. Marcuse, "Calculation of Bandwidth from Index Profiles of Optical Fibers. 1: Theory," Appl. Opt. *18* (June 1979), pp. 2073–2080.
9. E. A. J. Marcatili, "Modes in a Sequence of Thick Astigmatic Lens-Like Focusers," B.S.T.J., *43*, No. 6 (November 1964), pp. 2887–2904.
10. D. Gloge and E. A. J. Marcatili, "Multimode Theory of Graded-Core Fibers," B.S.T.J., *52* (November 1973), pp. 1563–1578.
11. R. Olshansky, "Propagation in Glass Optical Waveguides," Rev. Mod. Phys. *51* (April 1979), pp. 341–367.
12. A. Vigants and S. P. Schlesinger, "Surface Waves on Radially Inhomogeneous Cylinders," IEEE Trans., *MTT-10* (September 1962), pp. 375–382.
13. M. O. Vassel, "Calculation of Propagating Modes in a Graded Index Optical Fiber," Opto-Electronics, *6* (July 1974), pp. 271–386.

14. H. Kita, I. Kitano, T. Uchida, and M. Furakawa, "Light-Focusing Glass Fibers and Rods," J. Amer. Ceram. Soc., *54* (July 1971), pp. 321–326.
15. D. O. Smith, "Magneto-optical Scattering From Multilayer Magnetic and Dielectric Films," Optica Acta, *12* (January 1965), pp. 13–45.
16. Anthony Ralston, "Runge-Kutta Methods With Minimum Error Bounds," Mathematics of Computation, *16* (October 1962), pp. 431–437.
17. M. A. Gatto and Judith B. Seery, (unpublished work.)
18. J. W. Fleming, "Material and Mode Dispersion in $GeO_2 \cdot B_2O_3 \cdot SiO_2$ Glasses," J. Am. Ceram. Soc., *59* (November–December 1976), pp. 503–507.
19. J. W. Fleming, "Material Dispersion in Lightguide Glasses," Elec. Lett., *14* (May 1978), pp. 326–328.
20. M. Herzberger, *Handbook of Physics*, New York: McGraw-Hill, 1958, E. U. Condon and H. Odishaw, eds., pp. 6-42 to 6-43.
21. Albert E. Waugh, *Elements of Statistical Method*, New York: McGraw-Hill, 1952, pp. 446–448.
22. Wolfgang K. H. Panofsky and Melba Phillips, *Classical Electricity and Magnetism*, Boston: Addison-Wesley, 1958, pp. 161, 171, 198.
23. E. Bianciardi and V. Rizzoli, "Propagation in Graded-Core Fibers: A Unified Numerical Description," Optical and Quantum Electronics, *9* (March 1977), pp. 121–133.